Journal of Power Sources 195 (2010) 7684–7690

Contents lists available at ScienceDirect

Journal of Power Sources

journal homepage: www.elsevier.com/locate/jpowsour

Hybrid tandem solar cell for concurrently converting light and heat energy with utilization of full solar spectrum

Xiao-Zhi Guo, Yi-Duo Zhang, Da Qin, Yan-Hong Luo, Dong-Mei Li, Yu-Tong Pang, Qing-Bo Meng*

Beijing National Laboratory for Condensed Matter Physics, Institute of Physics, Chinese Academy of Sciences, Zhongguancun South Third Street 8, 100190 Beijing, China

ARTICLE INFO

Article history:
Received 22 March 2010
Received in revised form 14 May 2010
Accepted 19 May 2010
Available online 25 May 2010

Keywords:
Hybrid
Tandem
Dye-sensitized solar cells
Thermoelectric

ABSTRACT

A two-compartment hybrid tandem cell comprising a dye-sensitized solar cell as top cell and a thermoelectric cell as bottom cell has been developed to increase the overall photovoltaic conversion efficiency by utilization of full solar spectrum. The photovoltaic properties of the four-wire and two-wire hybrid tandem cells have been characterized and the working principle has been demonstrated using the electron energy band diagram. For two-wire hybrid tandem cells, the overall conversion efficiency can be improved by optimal designing DSC module in order to match the output current of the selected thermoelectric cell. Comparing with the individual dye-sensitized solar cell, an efficiency increase of 10% has been obtained for the hybrid tandem cell. The incident light intensity has no influence on the matching of the two compartments of the two-wire hybrid tandem cell.

1. Introduction

Dye-sensitized solar cells (DSCs) have currently been widely investigated since its low production cost and potentially high conversion efficiency [1–7]. They make use of the ability of molecular sensitizers to inject photoexcited electrons into the conduction band of wide band gap semiconductor materials and exhibit certified power conversion efficiencies over 11% [3–5]. Pursuing high efficiency is always the core task for photovoltaic devices. However, in the past few years, the efficiency of DSCs increased slowly. One major reason is that the commonly employed sensitizers are unable to make full use of the solar spectrum due to their low light-harvesting capacity in the long wavelength region.

The solar spectrum covers a wavelength region from 280 to 2700 nm, in which visible and infrared light occupy 44% and 53% radiant energy separately. However, the commonly employed sensitizers represented by N3 or N719 can only absorb solar light up to 800 nm, and the absorption coefficients of these dyes at the longer wavelength region (>600 nm) were not enough to catch photons efficiently. In order to overcome this limitation, one approach is to employ light scattering structures such as metal oxide particles with several hundreds nanometer diameter [8–10] or a photonic crystal [11] to enhance the light path length. Employing these scattering structures succeeded to enhance photocurrent by increasing light absorption at longer wavelength region ($600 < \lambda < 800$ nm), and all the reported DSCs with high efficiency have involved such structures. However, this cannot extend the spectral response to the wavelength longer than the absorption edge of the dye. The development of sensitizing dyes to extend absorption edge and to improve the overall photoelectric conversion efficiency has been another significant method in this field. Black dye with the widest absorption range by far, extends the absorption edge up to 1000 nm [12], but its absorption coefficient at the longer wavelength region is still very low, so it still does not meet the requirements of ideal sensitizer for a single junction photovoltaic cell converting standard global air mass 1.5 (AM 1.5) sunlight to electricity [13]. Adopting tandem design gives a promising approach. Kubo et al. developed a tandem cell containing two photovoltaic cells with different absorption wavelength complementary to each other [14–17]. In order to make low energy photons transmit through the upper compartment and be harvested by the lower one, the counter electrode of the upper cell must be transparent and no scatter structure should be used in it. Besides, the thickness of the TiO_2 layer in the upper compartment should be not more than 10 μm in order to reduce light loss. However, these strategies sacrificed the efficiency of upper cell. Recently, tandem pn-DSC has been realized in one cell by replacing the catalytic platinum layer with a dye-sensitized p-type semiconductor layer [18–21]. Unfortunately, photocurrent matching required the thickness of TiO_2 layer extremely thin [20], and the total conversion efficiency is not more than 2%.

During photoelectric conversion process in DSC, the power output is lower than the light energy absorbed by optical active substances (TiO_2 and sensitizers) and a considerable proportion of energy is lost through many ways. A big part of the wasted energy converts to heat leading temperature rise of DSC. Besides, photons with lower energy, which cannot take part in photoelectric con-

* Corresponding author. Tel.: +86 10 82649242; fax: +86 10 82649242.
E-mail address: qbmeng@iphy.ac.cn (Q.-B. Meng).

0378-7753/$ – see front matter © 2010 Elsevier B.V. All rights reserved.
doi:10.1016/j.jpowsour.2010.05.033

version, may be absorbed by non-optical active substances of DSC (such as glass, electrolyte, and cathode materials) and convert to heat too. As a result, the temperature of DSC working under irradiation of AM 1.5 sunlight can be as high as 60 °C or even higher, which is much higher than that of the environment [3]. Thermoelectricity with the advantages of vibrationless, noiseless, small, light, safe, reliable, long service life and environmentally friend, can make use of the temperature difference to generate electricity [22]. Combining thermoelectricity with DSC and utilizing the heat produced by DSC to generate electricity should improve the overall efficiency. Therefore, we report here a hybrid tandem cell (HTC) using a DSC and a piece-like thermoelectric cell (TC) as the upper and lower compartments, respectively. In the DSC, photons are absorbed by optical active and non-optical active materials, and the light energy is converted to electricity as well as heat. The heat then transmits to the TC and is used for thermoelectric conversion. By utilizing the heat which used to be lost in the past, HTC gives higher efficiency than a single DSC and realizes full-spectrum utilization.

2. Experimental

2.1. Preparation of DSC module

The DSC module was prepared as follows. First, the fluorine-doped tin oxide (FTO) layers on the FTO glass substrates were patterned by laser scribing. Then the TiO_2 photoelectrodes, the silver lines, and the platinum or carbon counter electrodes were screen printed successively on the respective FTO glass substrates. The TiO_2 electrodes were sensitized with cis-bis(iso-thiocyanato)-bis(2,2′-bipyridyl-4,4′-dicalboxylato)Ru(II)bis-tetrabutylammonium (N719). The liquid electrolyte is composed of 0.6 M methylhexylimidazolium iodide, 0.05 M iodine, 0.1 M LiI and 0.5 M tert-butylpyridine in 3-methoxypropionitrile. The DSCs were assembled according to Refs. [23,24].

2.2. Fabrication of HTC

The HTC was fabricated by sticking the back of the DSC module with the hot side of the TC (TECI-03180T125, Xiandai). The two compartments were both 40 mm × 40 mm in size.

2.3. Characterization and measurements

The transmittance and reflectance properties were obtained by UV–vis–NIR spectrophotometer (Lambda 19, PerkinElmer). The incident photon to current efficiency (IPCE) was measured by home-made IPCE setup, comprising xenon lamp (500 W, Changtuo), monochromator (λ-500, Anhe), current–voltage convert (home-made) and data storage equipment. The photocurrent–voltage measurements were recorded by a potentiostat (Model 263A, Princeton Applied Research). A solar light simulator (91192, Oriel) was used to mimic one sun AM 1.5 illumination on the surface of the solar cells. The intensity of incident light was measured with a radiant power/energy meter (70260, Oriel) before each experiment. The digital multimeter (8808A, Fluke) was used to record the current of each sub-cell during photocurrent–voltage measurement.

3. Results and discussion

3.1. UV–vis–NIR spectrum

Fig. 1 shows the optical characteristics of the FTO glass used in the DSCs. Absorption spectrum is obtained by employing Eq. (1). $T(\lambda)$, $R(\lambda)$ and $A(\lambda)$ represent transmittance, reflectance and absorbance of FTO glass at the wavelength of λ, respectively. The FTO glass shows a high transmittance above 80% in the visible region. With the extension of the wavelength to the infrared region, the transmittance decreases while the absorbance and reflectance increases significantly. In the region above 1500 nm, more than 40% of solar energy is absorbed by FTO glass.

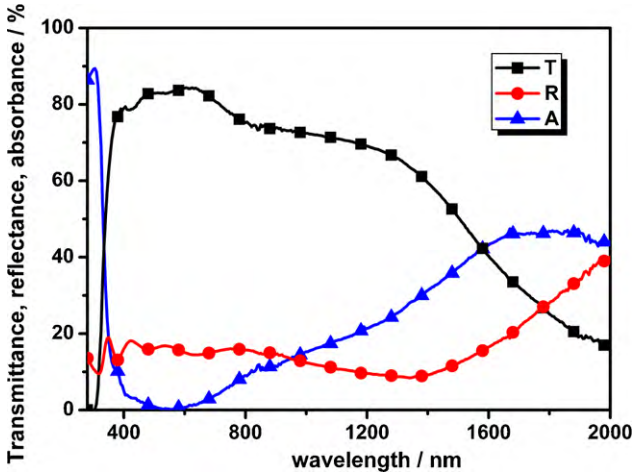

Fig. 1. Transmission (T), reflection (R) and absorption (A) spectra of the FTO glass.

$$T(\lambda) + R(\lambda) + A(\lambda) = 1 \quad (1)$$

The transmission, reflection and absorption spectra of DSCs are depicted in Fig. 2. DSC with platinum counter electrode just shows a low transmittance in the near infrared region. Almost 90% of the ultraviolet and visible light together with about 70% of the near infrared light is absorbed. For DSC with carbon counter electrode, scarcely any light can pass through, which denotes that the light is totally absorbed in addition to the part lost by reflex. Since carbon is inexpensive and full-spectrum absorption and its catalytic activity can match that of platinum [25–27], it is used as counter electrode in the following experiments.

Fig. 3 illustrates the utilization of solar energy by DSC from the perspective of solar spectrum. The energy lost by transmission and reflection $E_{T,R}(\lambda)$ was calculated as:

$$E_{T,R}(\lambda) = (T(\lambda) + R(\lambda)) \times E_{\text{solar}}(\lambda) \quad (2)$$

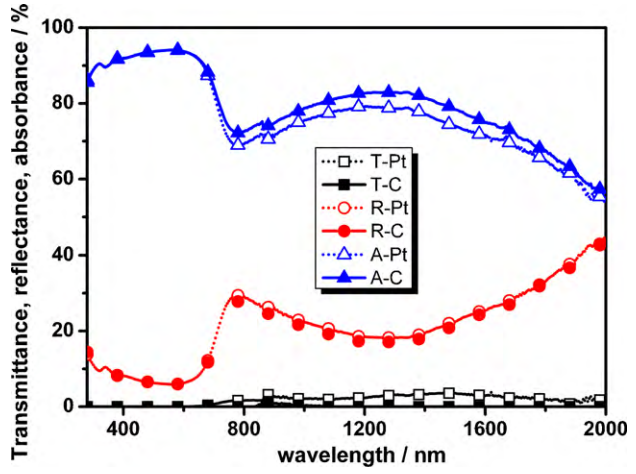

Fig. 2. Transmission (T), reflection (R) and absorption (A) spectra of DSCs with platinum (Pt) or carbon (C) counter electrode.

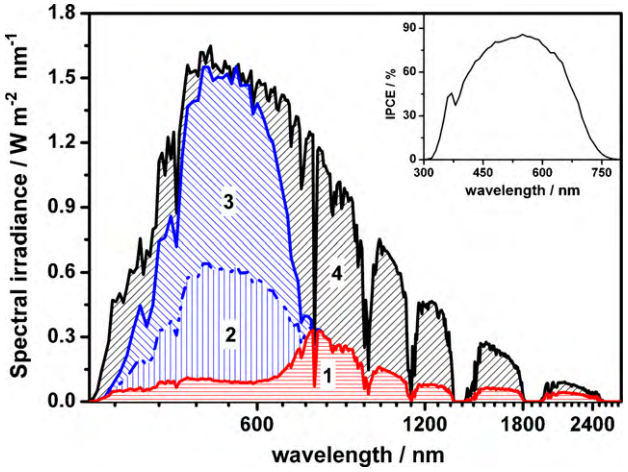

Fig. 3. Solar energy utilizing spectrum of DSC. Region 1: solar energy lost by reflection; region 2: solar energy absorbed by optical active substances and converted to electrical energy; region 3: solar energy absorbed by optical active substances but not converted to electrical energy; region 4: solar energy absorbed by non-optical active substances and converted to heat. The inset graph is the IPCE curve of DSC (aperture area = 0.2 cm^{-2}, photoelectric conversion efficiency = 8.3%).

$E_{solar}(\lambda)$ is the energy of solar radiation at the wavelength of λ. The energy absorbed by optical active substance $E_{abs}(\lambda)$ was calculated as:

$$E_{abs}(\lambda) = LHE(\lambda) \times E_{solar}(\lambda) \quad (3)$$

$LHE(\lambda)$ is light-harvesting efficiency. The incident photon to current efficiency ($IPCE(\lambda)$) of the cell was presented as:

$$IPCE(\lambda) = LHE(\lambda) \times \eta_{int}(\lambda) \times \eta_{cc}(\lambda) = LHE(\lambda) \times APCE(\lambda) \quad (4)$$

$\eta_{int}(\lambda)$ is electron injection quantum yield, $\eta_{cc}(\lambda)$ is charge collection efficiency, and $APCE(\lambda)$ is absorbed-photon conversion efficiency. For DSC with high efficiency, $\eta_{int}(\lambda)$ and $\eta_{cc}(\lambda)$ are unity [2,28–32], so Eq. (3) can be rewritten to:

$$E_{abs}(\lambda) \approx IPCE(\lambda) \times E_{solar}(\lambda) \quad (5)$$

From above calculation, we can see that among the energy of solar radiation, 15% is lost by transmission and reflection (Fig. 3 region 1), 27% is absorbed by optical active substances (Fig. 3 region 2 + region 3), while the remaining 58% (Fig. 3 region 4) of the solar energy is absorbed in the form of heat by non-optical active substances of DSC which cannot generate electricity. Even in the light energy absorbed by optical active substances, more than half is lost during photoelectric conversion. The electron exported from DSC contains electrical energy equivalent to qV, where q is charge of electron, V is the voltage between photoanode and cathode. While the energy of photon absorbed by TiO_2 or sensitizer is much higher than qV. The excess energy is lost during relaxation, interfacial charge transference and recombination process. Most of these excess energy converts to heat, and the remaining part converts to other forms of energy. This means that among the 85% of solar energy absorbed by DSC, at least 60% will convert to heat.

3.2. Four-wire HTC (HTC1)

3.2.1. Structure and working principle of HTC1

Figs. 4 and 5 show the schematic structure and corresponding electron energy band diagram of four-wire HTC (HTC1). In the HTC1, DSC and TC piled up and worked independently. With the DSC on the top, when light is applied on the glass side of HTC1, electrons are excited to a high energy state of the dye molecules and subsequently transferred to the conduction band of TiO_2. The original state of the dye is subsequently restored by electron donation from the electrolyte, an organic solvent containing iodide/triiodide couple. The regeneration of the sensitizer by iodide intercepts the recapture of the conduction band electron by the oxidized dye. The iodide is regenerated in turn by the reduction of triiodide at the counter electrode, and the circuit being completed via electron migration through the external load. The maximum voltage output of DSC (V_{DSC}) is dictated by the gap between the TiO_2's Fermi level ($E_{F,\ TiO_2-DSC}$) and the electrochemical potential of the electrolyte (Fig. 5(a)). In addition to the photoelectric conversion, DSC also produced heat and transferred it to the TC. The electron energy band structure of a TC is shown in prediction by only one thermocouple in Fig. 5(b). Once there is a temperature difference between the two sides of TC, carrier density of the semiconductor thermo-

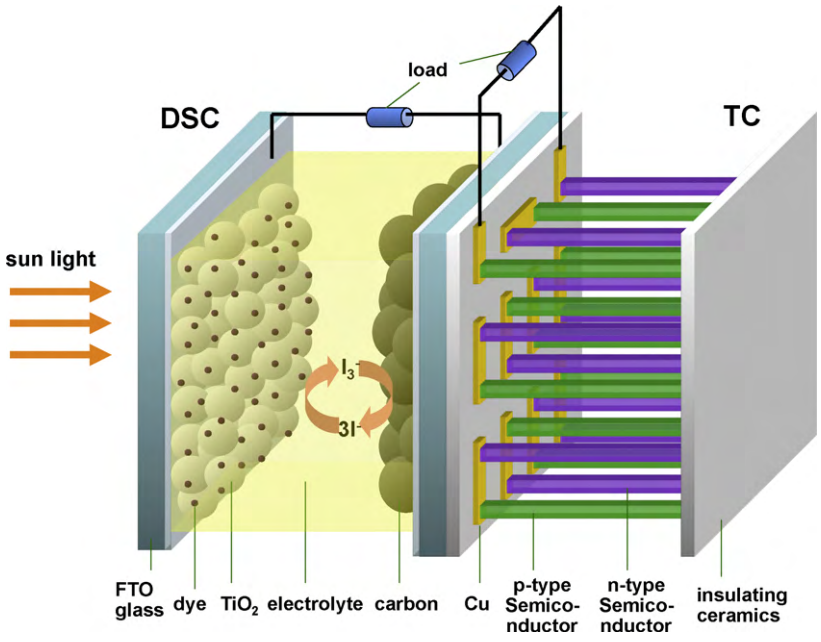

Fig. 4. Schematic structure of HTC1.

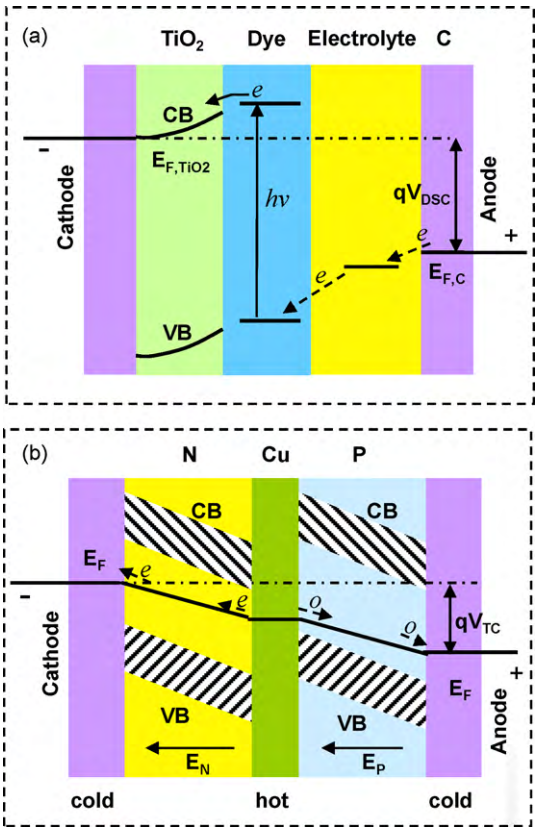

Fig. 5. Electron energy band diagrams of DSC (a) and TC (b). The abbreviations are as follows: conduction band (CB), valence band (VB), and Fermi level (E_F).

electric material is changed and the balance between diffusion and excursion of charge carriers is rebuilt, which drives the incline of Fermi level. The voltage output (V_{TC}) of TC is determined by the difference of the Fermi level at the anode and cathode.

3.2.2. Performance of HTC1

DSC module in parallel is easier preparation and widely used in research [23,33,34]. Therefore, we fabricated an all-parallel module with an overall size of 40 mm × 40 mm, and the details of this module are shown in Fig. 11(a). Under AM 1.5 100 mW cm^{-2} illumination, the DSC top cell yields a short circuit current of $I_{SC,DSC}$ = 120.0 mA, together with an open circuit voltage of $V_{OC,DSC}$ = 723 mV and a maximum power output of $P_{MAX,DSC}$ = 35.66 mW. In contrast, the corresponding parameters for the TC bottom cell are $I_{SC,TC}$ = 88.8 mA, $V_{OC,TC}$ = 192 mV, and $P_{MAX,TC}$ = 4.36 mW (Fig. 6). Due to the use of carbon as cathode material for DSC, light coming into the cell but not participating in photoelectric conversion, can be absorbed and transformed to heat entirely, causing temperature rise. According to the thermoelectric power generation characteristic of TC in Fig. 7, the temperature difference between the two sides of TC can be speculated as 17 °C due to the heat from DSC. The overall maximum output power of this HTC1 is $P_{MAX,HTC1} = P_{MAX,DSC} + P_{MAX,TC}$ = 40.02 mW, which is 11.2% higher than DSC alone.

3.3. Two-wire HTC (HTC2)

3.3.1. Structure and working principle of HTC2

The two-wire HTC (HTC2) was made by connecting DSC and TC in series. Fig. 8 gives its schematic structure, and the working principle can be explained using the electron energy band diagram shown in Fig. 9. After diffusing in the nanoporous film, electrons are

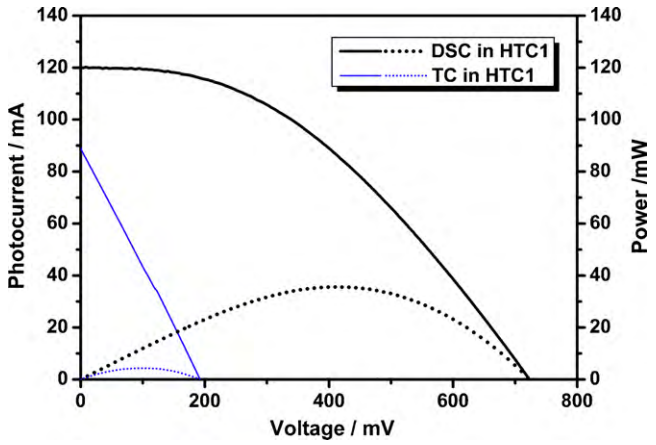

Fig. 6. Photocurrent–voltage (solid line) and power output (dot line) curves of HTC1.

exported through the cathode of DSC at the Fermi level $E_{F,\ TiO_2-DSC}$ and then captured by holes at the anode of TC. At the cathode of TC, electrons of the same amount are exported with higher energy. In the entire HTC2, the electron energy is promoted twice by TC and DSC.

3.3.2. Performance of HTC2

Using the same DSC module in HTC1, the overall maximum output voltage of HTC2 $V_{OC,HTC2}$ increased to 911 mV, which closely matches the sum of $V_{OC,DSC}$ (723 mV) and $V_{OC,TC}$ (192 mV). The short circuit current of HTC2 $I_{SC,HTC2}$ (119.4 mA) was almost unchanged comparing with $I_{SC,DSC}$ (120.0 mA), and a combined maximum output power $P_{MAX,HTC2}$ of 38.02 mW was obtained (Fig. 10). These experiment results are consistent with the theoretical ones (circles in Fig. 10) calculated from photocurrent–voltage curves of DSC and TC according to superposition theorem. In order to understand the working status of DSC and TC in HTC2, respectively, the photocurrent–voltage characteristics of these two compartments (squares in Fig. 10) were recorded simultaneously when the HTC2 was tested. The results showed highly agreement with the photocurrent–voltage curves of the two sub-cells under separate measurements, which indicates that the performance of DSC and TC remains unchanged after integration in HTC2.

3.3.3. Optimization of HTC2

The overall maximum power output of HTC2 with all-parallel DSC module $P_{MAX,HTC2}$ (38.02 mW) is lower than that of HTC1

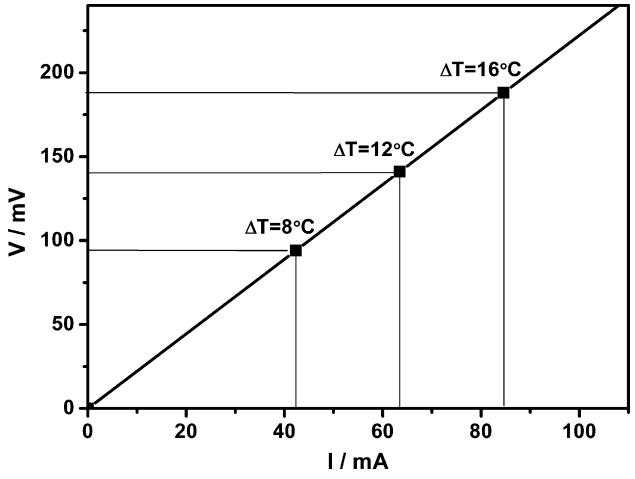

Fig. 7. Characteristic of thermoelectric power generation for TC.

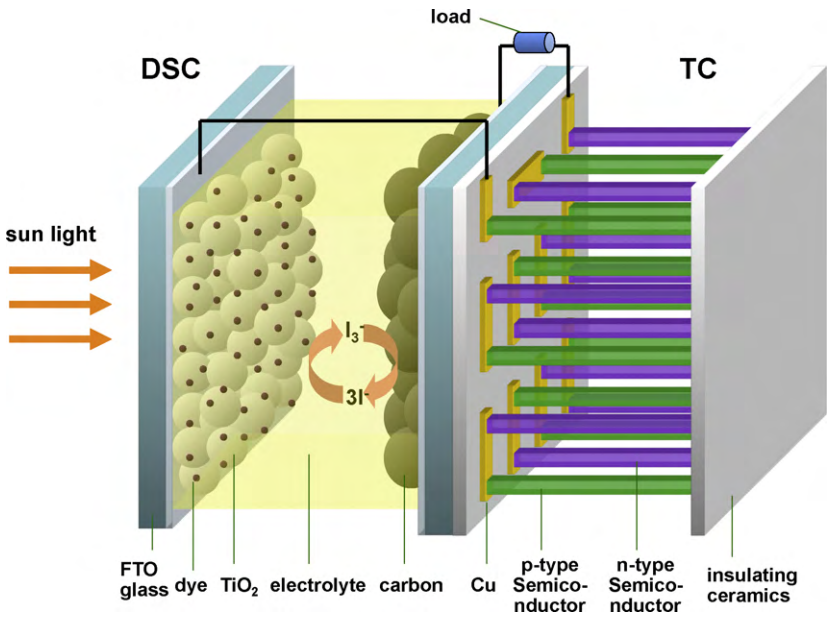

Fig. 8. Schematic structure of HTC2.

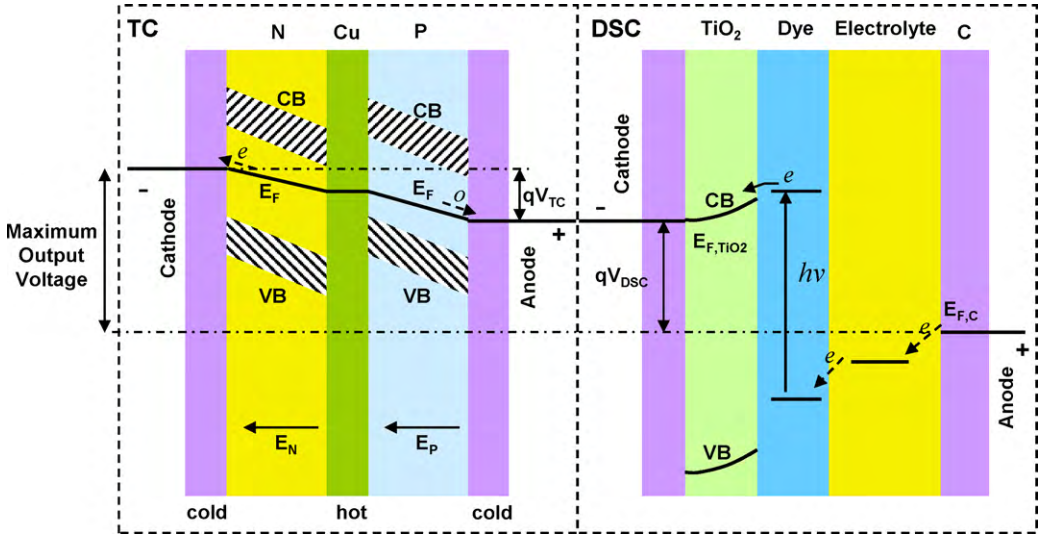

Fig. 9. Electron energy band diagram of HTC2.

($P_{MAX,HTC1} = P_{MAX,DSC} + P_{MAX,TC} = 40.02$ mW). This is because that the two compartments do not match to each other. In order to solve this problem and optimize the performance of HTC2, an attempt was made by designing different DSC modules. As shown in Fig. 11, three kinds of DSC modules with the same size of 40 mm × 40 mm were fabricated: DSC-a, all parallel; DSC-b, two series; DSC-c, three series. Photocurrent–voltage results of HTC2s with these DSC modules are shown in Fig. 12 and Tables 1 and 2. Since the DSC modules have the same size, the heat conducted from DSC to TC in HTC2s with different DSC modules is basically the same, and the performance of TC remains almost unchanged. The maximum power outputs of the three DSC modules are $P_{MAX,DSC-a} = 35.66$ mW, $P_{MAX,DSC-b} = 39.72$ mW and $P_{MAX,DSC-c} = 34.73$ mW, while the parameters of HTC2s with corresponding DSC module are $P_{MAX,HTC2-a} = 38.02$ mW, $P_{MAX,HTC2-b} = 44.26$ mW and $P_{MAX,HTC2-c} = 38.66$ mW, respectively. It can be seen from the data presented in Table 2 that the HTC2 assembled by DSC-b (HTC2-b) yields the largest increment of maximum power output of 4.54 mW and displays the best efficiency. Moreover, this increment is almost equal to the maximum power output of the TC component ($P_{MAX,TC} = 4.49$ mW). The above results can be explained as follows: the currents at the maximum output power points of DSC-b and TC are very close to each other

Table 1
Characteristics of HTCs with different DSC modules under AM 1.5 100 mW cm^{-2} illumination.

DSC module	Device		I_{SC} (mA)	V_{OC} (mV)	P_{MAX} (mW)
a	HTC1	DSC-a	120.0	723	35.66
		TC	88.9	192	4.48
	HTC2		119.4	911	38.02
b	HTC1	DSC-b	55.0	1394	39.72
		TC	88.8	192	4.49
	HTC2		54.7	1581	44.26
c	HTC1	DSC-c	36.6	2080	34.73
		TC	88.8	191	4.48
	HTC2		36.0	2268	38.66

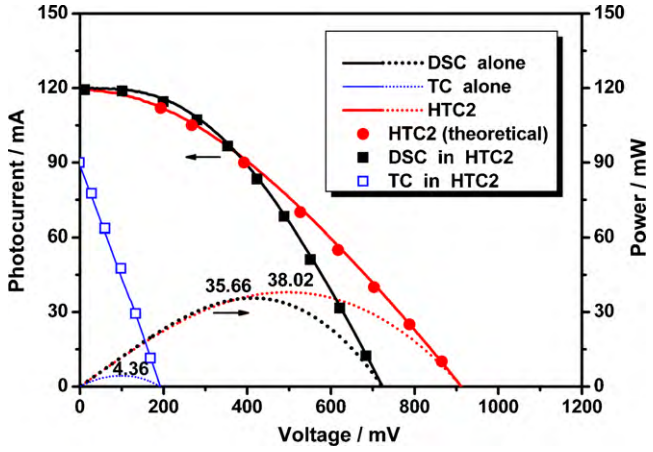

Fig. 10. Photocurrent–voltage (solid line) and power output (dot line) curves of HTC2 and its sub-cells under AM 1.5 100 mW cm^{-2} illumination. Circles are theoretical values of HTC2; squares are the working status of DSC (solid) and TC (hollow) while measuring HTC2.

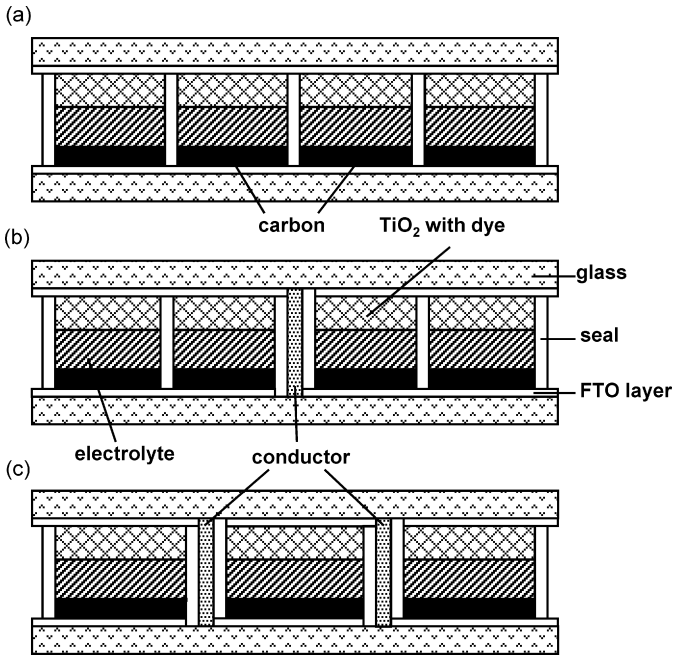

Fig. 11. Patterns of DSC modules: (a) all parallel; (b) two series; (c) three series.

Table 2
Current at the maximum power output point of HTC2s and the corresponding sub-cells under AM 1.5 100 mW cm^{-2} illumination, the increment of maximum power output after assemble are also shown in the last column.

DSC module	$I_{P_{MAX},DSC}$ (mA)	$I_{P_{MAX},TC}$ (mA)	$I_{P_{MAX},HTC}$ (mA)	ΔP_{MAX} (mW)
a	86.8	46.2	74.1	2.36
b	42.8	45.9	42.4	4.54
c	24.4	46.0	24.8	3.93

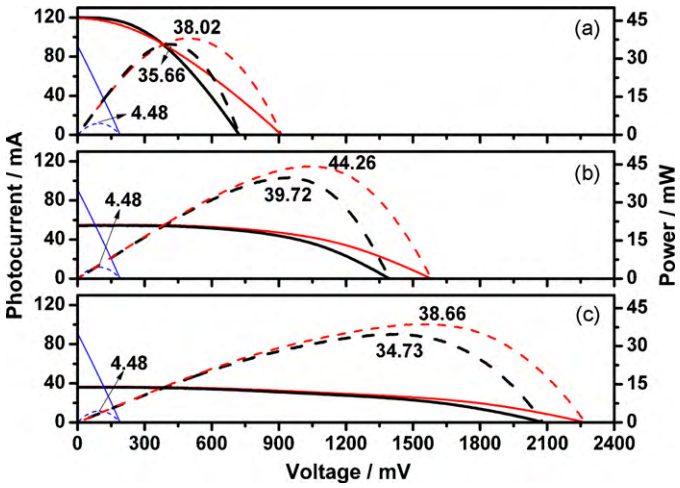

Fig. 12. Photocurrent–voltage (solid) and power output (dash) curves of HTC2 (red) with different DSC modules and the corresponding sub-cells (DSC: black, TC: blue) under AM 1.5 100 mW cm^{-2} illumination. (For interpretation of the references to color in this figure legend, the reader is referred to the web version of the article.)

($I_{P_{MAX},DSC-b}$ = 42.8 mA, $I_{P_{MAX},TC}$ = 46.2 mA), which makes it possible that the two sub-cells simultaneously work at their respective maximum power output point. For the HTC2 with DSC-a or DSC-c (HTC2-a or HTC2-c), the TC deviates from its own maximum power output point when the HTC2 output the largest power. The increment of the maximum power output is less than $P_{MAX,TC}$, due to the big disparity between $I_{P_{MAX},DSC}$ and $I_{P_{MAX},TC}$. It can be concluded that the DSC module used in HTC2 should be designed according to the photocurrent–voltage characteristic of the selected TC. The optimal power output of the HTC2, which is approximately equal to $P_{MAX,TC} + P_{MAX,DSC}$, can only be obtained when the currents of DSC and TC at their respective maximum power output point are almost the same.

3.4. Influence of incident light intensity

The photocurrent–voltage characteristics of HTC2-b and its sub-cells were tested under irradiation of different light intensity and the results are shown in Table 3 and Fig. 13. For DSC-b, the short circuit current $I_{SC,DSC-b}$ presents a linear relationship with light intensity and the open circuit voltage $V_{OC,DSC-b}$ increases with the increasing of light intensity, as is usually found in electrolyte-based dye-sensitized solar cells [35,36]. For the TC, both the short circuit current $I_{SC,TC}$ and the open circuit voltage $V_{OC,TC}$ increase with light intensity linearly, which indicates that the temperature difference of the two sides of TC also presents a linear relationship with incident light intensity. After integration in series, the short circuit current of HTC2-b ($I_{SC,HTC2-b}$) is almost the same with $I_{SC,DSC-b}$, and the open circuit voltage ($V_{OC,HTC2-b}$) equals to the sum of $V_{OC,DSC-b}$ and $V_{OC,TC}$ no matter how strong the incident light intensity is. As shown in Fig. 13(a), the approximately equal relationship between $I_{P_{MAX},DSC-b}$ and $I_{P_{MAX},TC}$ is maintained under irradiation of different light intensity. This indicates that once the matching between DSC

Table 3
Characteristics of HTC2-b and its sub-cells under irradiation of different light intensity.

Light intensity (mW cm^{-2})	I_{SC} (mA)			V_{OC} (mV)			P_{MAX} (mW)		
	DSC-b	TC	HTC2-b	DSC-b	TC	HTC2-b	DSC-b	TC	HTC2-b
20	11.7	19.3	12.4	1314	40.3	1365	10.82	0.20	11.15
40	22.8	35.4	23.4	1345	73.3	1431	20.26	0.66	20.88
70	39. 9	62.1	40.2	1376	129.9	1516	32.75	2.09	34.43
100	57.0	95.2	56.7	1407	178.4	1579	41.30	3.94	45.40

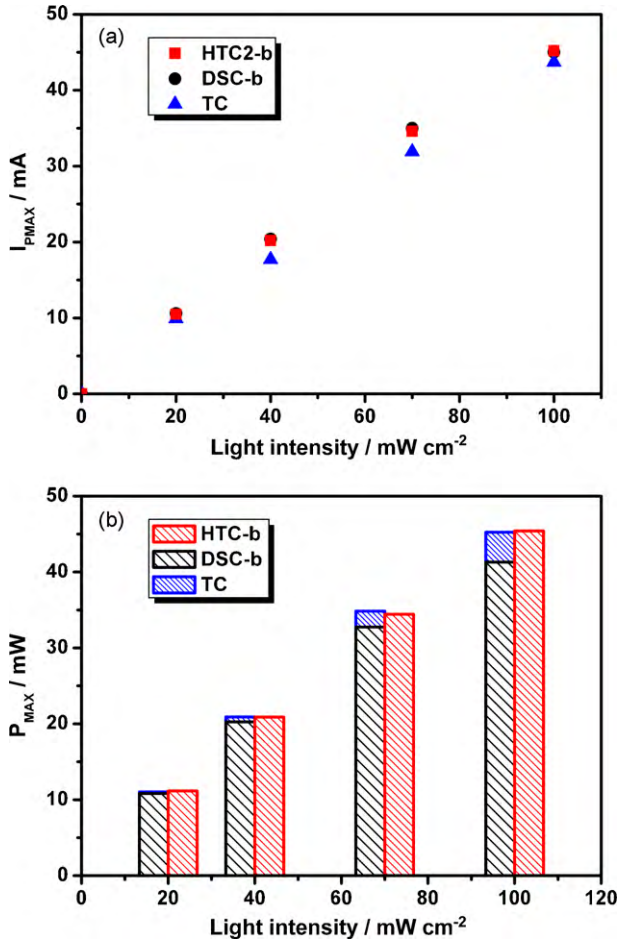

Fig. 13. Matching effect between the two sub-cells in HTC2-b under irradiation of different light intensity: (a) current at the maximum power output point (I_{PMAX}); (b) maximum power output (P_{MAX}).

and TC is achieved, it will not be affected by the incident light intensity, so the maximum power output of the whole cell will always be approximately equal to the sum of the maximum output power of each compartment, which is in agreement with the experimental results (Fig. 13(b)).

4. Conclusions

The energy conversion in a high efficiency DSC is analyzed from the perspective of solar energy spectrum. Up to 85% of solar energy is absorbed by DSC and more than 60% of which converts to heat instead of electrical energy. A method which could simultaneously convert the heat produced by DSC to electricity is urgently desired for fully utilizing the solar energy. Here, HTC is successfully designed and fabricated for combining thermoelectric conversion with photoelectric conversion by assembling an HTC with a DSC and a piece-like TC as the upper and lower compartments, respectively. In the HTC, DSC absorbs photon and generates electricity and heat, while the TC re-uses this heat and generates electricity. The two sub-cells can work simultaneously or individually. By optimizing design of the DSC module, photocurrent matching of the two compartments of HTC integrated in serial is achieved, and the overall conversion efficiency increased by 10% compared with a single DSC. The present approach achieves photocurrent matching by designing the series–parallel mode of DSC rather than changing its microstructure, so there is little effect on the efficiency of DSC itself. Our study demonstrates a new concept of concurrently converting light and heat using a hybrid cell so that the solar energy can be effectively and full-spectrum utilized. Further efficiency increases can be achieved by improving the efficiency of DSC and/or TC.

Acknowledgements

This work was supported by the National Natural Science Foundation of China (Nos. 20725311, 20673141, 20703063, 20721140647 and 20873178), the Ministry of Science and Technology of China (973, Project No. 2006CB202606 and 863, Project No. 2006AA03Z341) and Knowledge Innovation Project of The Chinese Academy of Sciences.

References

[1] B. O'Regan, M. Grätzel, Nature 353 (1991) 737–740.
[2] M.K. Nazeerudin, A. Kay, I. Rodicio, R. Huxnpbry-Baker, E. Miiller, P. Liska, et al., J. Am. Chem. Soc. 115 (1993) 6382–6390.
[3] M. Grätzel, J. Photochem. Photobiol. A 164 (2004) 3–14.
[4] Y. Chiba, A. Islam, Y. Watanabe, R. Komiya, N. Koide, L. Han, Jpn. J. Appl. Phys. 45 (2006) 638–640.
[5] F. Gao, Y. Wang, D. Shi, J. Zhang, M. Wang, X. Jing, R.H. Baker, P. Wang, S.M. Zakeeruddin, M. Grätzel, J. Am. Chem. Soc. 130 (2008) 10720–10728.
[6] A.J. Frank, N. Kopidakis, J. van de Lagemaat, Coord. Chem. Rev. 248 (2004) 1165–1179.
[7] P.V.V. Jayaweera, A.G.U. Perera, K. Tennakone, Inorg. Chim. Acta 361 (2008) 707–711.
[8] A. Usami, Chem. Phys. Lett. 277 (1997) 105–108.
[9] X. Liu, Q. Meng, C. Gao, B. Xue, H. Wang, L. Chen, O. Sato, A. Fujishima, Chin. Phys. Lett. 21 (2004) 1384–1387.
[10] Z. Wang, H. Kawauchi, T. Kashima, H. Arakawa, Coord. Chem. Rev. 248 (2004) 1381–1389.
[11] S. Nishimura, N. Abrams, B.A. Lewis, L.I. Halaoui, T.E. Mallouk, K.D. Benkstein, J. van de Lagemaat, A.J. Frank, J. Am. Chem. Soc. 125 (2003) 6306–6310.
[12] M.K. Nazeeruddin, P. Péchy, T. Renouard, S.M. Zakeeruddin, R. Humphry-Baker, P. Comte, P. Liska, L. Cevey, E. Costa, V. Shklover, L. Spiccia, G.B. Deacon, C.A. Bignozzi, M. Grätzel, J. Am. Chem. Soc. 123 (2001) 1613–1624.
[13] M. Grätzel, J. Photochem. Photobiol. C 4 (2003) 145–153.
[14] W. Kubo, A. Sakamoto, T. Kitamura, Y. Wada, S. Yanagida, J. Photochem. Photobiol. A 164 (2004) 33–39.
[15] M. Dürr, A. Bamedi, A. Yasuda, G. Nelles, Appl. Phys. Lett. 84 (2004) 3397–3399.
[16] P. Liska, K.R. Thampi, M. Grätzel, D. Brémaud, D. Rudmann, H.M. Upadhyaya, A.N. Tiwari, Appl. Phys. Lett. 88 (2006) 203103-1–203103-3.
[17] M. Murayama, T. Mori, J. Phys. D: Appl. Phys. 40 (2007) 1664–1668.
[18] J. He, H. Lindstro, A. Hagfeldt, S.E. Lindquist, J. Phys. Chem. B 103 (1999) 8940–8943.
[19] J. He, H. Lindström, A. Hagfeldt, S.E. Lindquist, Sol. Energy Mater. Sol. Cells 62 (2000) 265–273.
[20] A. Nattestad, A.J. Mozer, M.K.R. Fischer, Y.B. Cheng, A. Mishra, P. Bäuerle, U. Bach, Nat. Mater. 9 (2010) 31–35.
[21] A. Nattestad, M. Ferguson, R. Kerr, Y.B. Cheng, U. Bach, Nanotechnology 19 (2008) 295304.
[22] D.M. Rowe, Renew. Energ. 16 (1999) 1251–1256.
[23] M. Späth, P.M. Sommeling, J.A.M. van Roosmalen, H.J.P. Smit, N.P.G. van der Burg, D.R. Mahieu, N.J. Bakker, J.M. Kroon, Prog. Photovolt.: Res. Appl. 11 (2003) 207–220.
[24] X. Pan, S.Y. Dai, K.J. Wang, L.H. Hu, C.W. Shi, L. Guo, F.T. Kong, Chin. J. Chem. 23 (2005) 1579–1583.
[25] Z. Huang, X. Liu, K. Li, D. Li, Y. Luo, H. Li, W. Song, L. Chen, Q. Meng, Electrochem. Commun. 9 (2007) 596–598.
[26] K. Li, Z. Yu, Y. Luo, D. Li, Q. Meng, J. Mater. Sci. Technol. 23 (2007) 577–582.
[27] J. Chen, K. Li, Y. Luo, X. Guo, D. Li, M. Deng, S. Huang, Q. Meng, Carbon 47 (2009) 2704–2708.
[28] M. Grätzel, Inorg. Chem. 44 (2005) 6841–6851.
[29] T. Trupke, P. Wulrfel, J. Phys. Chem. B 104 (2000) 11484–11488.
[30] M.K. Nazeeruddin, F. de Angelis, S. Fantacci, A. Selloni, G. Viscardi, P. Liska, S. Ito, B. Takeru, M. Grätzel, J. Am. Chem. Soc. 127 (2005) 16835–16847.
[31] S.M. Waita, J.M. Mwabora, B.O. Aduda, G.A. Niklasson, S.E. Lindquist, C.G. Granqvist, AJST 7 (2006) 106–119.
[32] Y. Tachibana, H. Hara, K. Sayama, H. Arakawa, Chem. Mater. 14 (2002) 2527–2535.
[33] S.Y. Dai, J. Weng, Y. Sui, C. Shi, Y. Huang, S. Chen, X. Pan, X. Fang, L. Hu, F. Kong, Sol. Energy Mater. Sol. Cells 84 (2004) 1–4.
[34] Y. Huang, S.Y. Dai, S. Chen, C. Zhang, Y. Sai, S. Xiao, L. Hu, Appl. Phys. Lett. 95 (2009) 243503-1–243503-3.
[35] S. Södergren, A. Hagfeldt, J. Olsson, S.E. Lindquist, J. Phys. Chem. 98 (1994) 5552–5556.
[36] F. Cao, G. Oskam, G.J. Meyer, P.C. Searson, J. Phys. Chem. 100 (1996) 17021–17027.